Revision 2

# A high-pressure, clinopyroxene-structured polymorph of albite in highly shocked terrestrial and meteoritic rocks

CHI MA[1,*], OLIVER TSCHAUNER[2], MIHYE KONG[3,†], JOHN R. BECKETT[1], ERAN GREENBERG[4], VITALI B. PRAKAPENKA[4], YONGJAE LEE[3]

[1]Division of Geological and Planetary Sciences, California Institute of Technology, Pasadena, CA 91125, USA
[2]Department of Geoscience, University of Nevada, Las Vegas, NV 89154, USA
[3]Department of Earth System Sciences, Yonsei University, Seoul 03722, Republic of Korea
[4]GSECARS, University of Chicago, Argonne National Laboratory, Chicago, IL 60637, USA
[†]Present address: Interdisciplinary Materials Measurement Institute, Korea Research Institute of Standards and Science, Daejeon 34113, Republic of Korea

## ABSTRACT

Clinopyroxenes with excess Si have been described in run products from high-pressure experiments and inferred to have existed in nature from retrograde transformation phases. Here, we present the discovery of albitic jadeite, $(Na,Ca,\square_{¼})(Al,Si)Si_2O_6$ - the first natural, sodic clinopyroxene with excess Si occupying the octahedral cation site, M1, and a corresponding ¼ vacancy on the M2-site in the Ries impact structure and in a suite of L6 ordinary chondrites, EET 13014, EET 13052, NWA 1662, and TIL 08001. Garnet compositions in these samples indicate shock pressures of 18 - 22 GPa. Based on our survey, albitic jadeite is likely to be rather common in terrestrial and meteoritic shock-metamorphic environments. Shock-generated jadeite should be reexamined with respect to excess Si.

**Keywords**: albitic jadeite, $(Na,Ca,\square_{¼})(Al,Si)Si_2O_6$, high-pressure clinopyroxene, shock-induced phase, Ries impact structure, L6 ordinary chondrites.

*E-mail: chima@caltech.edu

## INTRODUCTION

At low pressures, Si exclusively occupies tetrahedral sites in clinopyroxene. A compositional analysis that indicates more Si than can be accomodated in tetrahedral coordination generally reflects a poor analysis or contamination of the analytical volume by some other phase. However, clinopyroxenes that were synthesized in high-pressure experiments clearly exhibit Si, not only on the tetrahedral, but also on the octahedral M1 site. Charge-balancing of excess Si is usually achieved through compensating vacancies on the M2 site (e.g., Angel et al. 1988; Liou et al. 1998), although octahedral vacancies at high pressure can also be mediated by Al (e.g., Wood and Henderson 1978; Ma et al. 2015). Regardless of the actual mechanism, increasing vacancies on the M2 site with increasing depth has been proposed to play an important role in the distribution water in the sublithospheric mantle (e.g., Bell and Rossman 1992; Warren and Hauri 2014).

The presence of octahedral Si in clinopyroxene equilibrated at high pressures is well established by direct observations on synthetic clinopyroxenes (e.g., Angel et al. 1988; Yang et al. 2009). The case for octahedral Si in natural pyroxenes is less direct. There is no evidence, for example, that omphacite, the dominant pyroxene in subducted slabs, contains octahedrally coordinated Si. Omphacite phenocrysts from some exhumed ultahigh-pressure metamorphic terrains do, however, exhibit orientated lamellae of quartz or coesite and these lamellae are often interpreted to be the exsolution products of a former excess Si component upon exhumation and indicative of the high peak pressures experienced by these rocks (e.g., Zhang et al. 2005).

In static high-pressure, high-temperature experiments, albite ($NaAlSi_3O_8$) breaks down to form jadeite ($NaAlSi_2O_6$) and a dense $SiO_2$ phase, either coesite or stishovite (e.g., Liu 1978). On Earth, the formation of jadeite ($NaAlSi_2O_6$) through dissociation of albitic plagioclase in metapelites or basalt marks the onset of eclogitization in high-pressure metamorphic environments. The same reaction has also been reported from shocked ordinary chondrites (e.g., Tropper et al. 1999, Miyahara et al. 2013). Here, we report a new vacancy-stabilized, high-pressure, high-temperature clinopyroxene with Si on the M1 site and a composition essentially equivalent to that of albitic plagioclase. This clinopyroxene is formed by shock metamorphic transformation of albite in terrestrial impactites and ordinary chondrites. It has not been previously observed or synthesized and, therefore, it provides potential new insights into shock conditions and impact processes.

We examined an amphibolite xenolith from suevite of the Ries impact structure and the L6 ordinary chondrites EET 13014, EET 13052, TIL 08001, and NWA 1662 with advanced electron-beam and synchrotron techniques, and discovered a highly-defective, shocked-induced, high-pressure albitic jadeite (Figs. 1-2). The new phase is an Na-analog of tissintite ($(Ca,Na,\square_{1/4})Al(Si,Al)_2O_6$), and has a structural formula of $(Na,Ca,\square_{1/4})(Al,Si)Si_2O_6$. Its composition ranges from $(Na_{0.75}\square_{0.25})(Al_{0.75}Si_{0.25})Si_2O_6$ to $(Na_{0.50}Ca_{0.25}\square_{0.25})AlSi_2O_6$, which corresponds to plagioclase with An0-An33 compositions. A clinopyroxene with this structure exhibits a high concentration of excess Si on the octahedral cation M1 site and an M2 site with ¼ vacancy. This clinopyroxene is a new high-pressure phase, a polymorph of albite, but it is still a "jadeite" – not a new mineral – according to the dominant-constituent and dominant-valency rules of the IMA-CNMNC (Hatert and Burke 2008). In particular, it is a supersilicic jadeite with albite composition, which we label as "albitic jadeite" in reference to its formation via solid-solid transformation of precursor albite and to distinguish it from synthetic jadeites with excess Si. Ma et al. (2020) give a preliminary description of albitic jadeite, which is expanded on in this study.

## SAMPLES AND ANALYTICAL METHODS

A thin section of amphibolite xenolith ZLN100 from the Ries impact structure and a thin section of the L6 chondrite NWA 1662 are from the Museum für Naturkunde Berlin, those of EET 13014 and EET 13052 from Yonsei University, and TIL 08001 from the Korea Polar Research Institute. Field-emission scanning electron microscope (FE-SEM), energy-dispersive X-ray spectroscopy (EDS), electron back-scatter diffraction (EBSD), electron probe microanalysis (EPMA), and synchrotron X-ray diffraction were used to characterize the composition, structure and petrography of albitic jadeite and associated phases. Back-scatter electron (BSE) imaging was performed using a ZEISS 1550VP FE-SEM. EBSD analyses were carried out using an HKL EBSD system on a ZEISS 1550VP SEM, operated at 20 kV and 6 nA in focused-beam mode with a 70º tilted stage and variable pressure mode (25 Pa). Chemical analyses were carried out using a JEOL 8200 electron probe at 15 kV and 10 nA with a probe diameter of ~150 nm and an Oxford X-Max SDD EDS on the ZEISS 1550VP SEM at 10 kV and 15 kV.

Synchrotron diffraction data were collected at the undulator beamline 16-IDB (HPCAT, APS, Argonne National Laboratory) using a beam of wavelength 0.31856 Å,

focused with elliptical mirrors to 2×3 μm² vertical and horizontal dimensions. A PILATUS 1M hybrid pixel array detector was used for data acquisition. Diffraction patterns were collected in forward scattering geometry over a grid across regions with albitic jadeite (e.g., Figs. 1-2) with 10 μm steps; the sample was oscillated by ± 20° around the ϕ-axis during data acquisition of 10 s. The diffraction patterns of albitic jadeite are powder-like with smooth Debye fringes. Patterns from EET 13014, EET 13052 and TIL 08001 exhibited strong contributions from coarse-grained, host rock mineral phases underneath the albitic material exposed at the surface of the thin section and were not suitable for structural analysis but contained some evidence for the presence of albitic jadeite. Patterns from the Ries xenolith ZLN100 showed varying contributions of fine-grained garnet and albitic jadeite and were used for Rietveld refinement. Diffraction frames were calibrated and integrated with the DIOPTAS software (Prescher and Prakapenka 2015). A diffraction frame without noticeable orientation of crystallites was choosen for Rietveld refinement (Fig. 3). The starting model of clinopyroxene was generated from jadeite (Table S1) but, initially, with full occupancy of the M2 site. For garnet, site occupancies were initially adjusted to match the EPMA composition and unit cell dimensions were manually adjusted to match the observed reflections prior to refinement. No deviation from the cubic metric was resolvable. Validity of the structure models was checked for both phases through reversed Monte Carlo modeling based on extracted |F(hkl)|. For garnet, the average electron densities of the X- and Y-sites were examined by local optimization using procedures described in Huang et al. (2020). The relative electron density per site was partitioned among the elements present and this site distribution was used in the Rietveld refinement. The rMC modeling converged to $R_F$ = 13.8% and Rietveld refinement (Kraus and Nolze 1996) converged to $R_{wp}$=12.61, $R_p$=9.54. The examined pattern gave 24 ± 3 vol.% clinopyroxene and 76 ± 3 vol.% garnet (Fig. 3). The Le Bail extraction converged to $R_p$=5.95. Gaussian profile terms for clinopyroxene and garnet were U = 0.655, V = 0.010, W = 0.0065 and U = 0.530, V = 0.0079, W = 0.0025, respectively, with an initial Lorentzian mixing term converging to zero for each phase. An additional Rietveld refinement of the three added patterns of textured material with GSAS (Larson and Von Dreele 2004) converged to $R_{wp}$ = 10.06%, $R_p$ = 7.4, $\chi^2$ = 2.2 for 1414 observation and the $R_{F2}$ were 16.7 and 11.2% for clinopyroxene and garnet, respectively.

## RESULTS

Albitic jadeite occurs as aggregates crystallized from maskelynite within, or in contact with, shock melt veins (Figs. 1-2). The amphibolite xenolith ZLN100 from the Ries suevite has been characterized by Stähle et al. (2011, 2017). It consists of pargasitic amphibole (Stähle et al. 2011) and maskelynite ($An_{66}Ab_{33}Or_1$ and $An_4Ab_{94}Or_1$), with minor titanite, clinozoisite, and rare magnetite, apatite, and Fe-sulfide and is crosscut by a 50-500 μm thick melt vein. In section, albitic jadeite occurs within ~5-10 μm of a contact between sodic maskelynite and the shock melt vein (note that the observed distances in section are maxima because the plane of a thin section generally doesn't capture the closest approach between two objects). It also forms aggregates of subhedral 100-800 nm crystals within the shock melt vein, surrounded by euhedral garnet (Fig. 1). Here, the albitic jadeite grains are pseudomorphs after clasts of albite that were trapped in the melt but not digested.

Unit cell parameters of albitic jadeite with the *C*2/*c* diopside-type structure in Ries ZNL100 were refined by synchrotron X-ray diffraction to $a = 9.442 \pm 2$ Å, $b = 8.606 \pm 2$ Å, $c = 5.253 \pm 1$Å and ß = 107.47 ± 2°, where quoted errors are 1σ, and found to range between 9.424 - 9.455 Å, 8.589 - 8.606 Å, 5.216 - 5.253 Å, and 107.72° - 107.45°, for all analyzed data from ZLN100. The unit cell length of the garnet was $a = 11.632 \pm 0.001$ Å. Fractional atomic coordinates, site fractional occupancies, and isotropic thermal displacement factors of albitic jadeite and garnet from Ries are given in Table S2. The composition of clinopyroxene in the shock melt vein from Ries (Table 1) yields an empirical formula based on 6 O *apfu* of $(Na_{0.65}Ca_{0.04}K_{0.04}Mg_{0.01}\square_{0.25})(Al_{0.80}Si_{0.19}Fe_{0.01})Si_2O_6$ with a general formula of $(Na,Ca,\square_{1/4})(Al,Si)Si_2O_6$, a composition that is also consistent with an albite precursor $(Na_{0.87}Ca_{0.05}K_{0.05}Mg_{0.01}Fe_{0.01})(Si_{2.92}Al_{1.07})O_8$ (i.e., this is an albitic jadeite). Vacancies occupy about 25% of the Na-dominant M2-site and excess Si ~20% of the Al-dominant octahedral M1-site. Trace K occurs along with Na and Ca on the M2-site. Albitic jadeite is electron beam sensitive (analysis invariably produces a mark/hole), likely due to metastability of excess Si in the M1 site under ambient conditions. This makes the acquisition of an EBSD pattern difficult to obtain, although not impossible. Figure 4 shows one of the best EBSD patterns we obtained for albitic jadeite (NWA 1662). Beam sensitivity also provides an important identifying contrast with natural jadeites that contain no excess Si, which are rather insensitive to the electron beam.

160 The surrounding euhedral garnet of the melt vein in ZLN100 (Table 1; Fig. 1) has an
161 empirical formula based on 12 O *apfu* of
162 $(Mg_{0.94}Ca_{0.82}Fe_{0.74}Na_{0.34}K_{0.03}Mn_{0.01})(Al_{1.49}Si_{0.48}Ti_{0.05})Si_3O_{12}$ with excess Si on the octahedral
163 *Y*-site and pyrope (Pyr), almandine (Alm), grossular (Gro) and hypothertical
164 $(Na_2Ca)Si_2Si_3O_{12}$ (NSS) as the main components, i.e., $\sim Pyr_{31}Alm_{25}NSS_{25}Gro_{19}$.
165 TIL 08001, EET 13014, EET 13052 and NWA 1662 are L6 ordinary chondrites that
166 experienced S3-S6 level shock metamorphism (Meteoritical Bulletin Database), which led to
167 undulose extinction in olivine, albite transformed into maskelynite, and the presence of
168 wadsleyite, majoritic garnet, and albitic jadeite as high-pressure minerals (Fig. 2); the shock-
169 produced phases were identified through BSE imaging, EDS, and EBSD.
170 In TIL 08001, albitic jadeite crystallizes in albitic maskelynite adjacent to shock-melt
171 veins (Fig. 2a), similar to the growth of tissintite in maskelynite of much more calcic
172 plagioclase composition in the Tissint martian meteorite (Ma et al. 2015). The empirical
173 formula of albitic jadeite in TIL 08001 by EDS is $\sim(Na_{0.54}Ca_{0.08}K_{0.04}\square_{0.32})(Al_{0.8}Si_{0.2})Si_2O_6$,
174 where ~ is used to emphasize the approximate nature of the alkali content, with > ¼
175 vacancies in M2 due to apparent Na-diffusion away from the electron beam. The composition
176 of wadsleyite in TIL 08001 is $(Mg_{1.49}Fe_{0.51})SiO_4$.
177 We observed an occurrence of albitic jadeite formed in albitic maskelynite within one
178 shock melt vein in EET 13014 (Fig. 2b) with a composition of
179 $\sim(Na_{0.59}Ca_{0.08}K_{0.06})(Al_{0.82}Si_{0.16}Fe_{0.03})Si_2O_6$. The composition of associated majoritic garnet is
180 $(Mg_{2.03}Fe_{0.65}Na_{0.25}Ca_{0.07})(Al_{0.81}Si_{0.68}Mg_{0.51})Si_3O_{12}$ and the compsition of ferropericlase is
181 $(Mg_{0.56}Fe_{0.44})O$. The composition of wadsleyite is $(Mg_{1.45}Fe_{0.54}Mn_{0.01})SiO_4$.
182 In EET 13052, albitic jadeite, which formed from maskelynite within one shock melt
183 vein (Fig. 2c), has a composition of $\sim(Na_{0.59}Ca_{0.08}K_{0.04})(Al_{0.77}Si_{0.23})Si_2O_6$. The compositions
184 of associated majoritic garnet and wadsleyite are
185 $(Mg_{2.02}Fe_{0.78}Na_{0.15}Ca_{0.06})(Al_{0.68}Si_{0.72}Mg_{0.60})Si_3O_{12}$ and $(Mg_{1.17}Fe_{0.83})SiO_4$, respectively.
186 Albitic jadeite in maskelynite at the edge of a shock melt vein in NWA 1662 (Fig. 2d)
187 has a composition of $\sim(Na_{0.57}Ca_{0.08}K_{0.03})(Al_{0.84}Si_{0.16})Si_2O_6$. The composition of wadsleyite is
188 $(Mg_{1.48}Fe_{0.50}Mn_{0.01})SiO_4$.
189

## DISCUSSION

Shock-induced phases and their compositions can be used to constrain the conditions of a shock event. For example, the pressure experienced by the Ries amphibolite ZNL100 can be estimated from the majorite-component of the garnet (see Collerson et al. 2010), which yields a pressure range of 18 – 22 GPa. This pressure range is consistent with the solid-solid transformation of amphibole at the rim of the melt vein (19 - 21 GPa), the observed polymorphs of titania (Tschauner et al. 2019; ~20 GPa), and the formation of stöfflerite (Tschauner et al. 2021; ~20 GPa). It is also in agreement with the fact that about half of the host-rock plagioclase is fully transformed to maskelynite (Stähle et al. 2017). In contrast, compositions of garnets in the chondrites EET 13014, EET 13052, and NWA 1662 indicate pressures of formation of ~ 22 Gpa, using Collerson et al. (2010), whereas the presence of wadsleyite suggests shock pressures to 14 - 18 GPa. This is consistent with a generally observed wide range of apparent shock levels within individual meteorites (Sharp and DeCarli 2006).

Albitic jadeite is a new high-pressure polymorph of albite joining lingunite, which is $NaAlSi_3O_8$ in the hollandite-type structure and it forms under similar conditions (Gillet et al. 2000). Under static high pressures, these phases may only exist in the form of minor components in jadeite, but in terrestrial impactites and shocked meteorites, such pyroxenes may be common. Albitic jadeite forms through the reaction:

$$3\ NaAlSi_3O_8 \rightarrow 4\ (Na_{0.75}\square_{0.25})(Al_{0.75}Si_{0.25})Si_2O_6.$$

The endmember formula is conventionally broken down to 3/4 $NaAlSi_2O_6$ (jadeite) + 1/4 $\square SiSi_2O_6$ (hypothetical clinopyroxene endmember with octahedral Si). Since the jadeite component dominates, this phase is an albitic jadeite and does not define a new mineral. Nevertheless, albitic jadeite adds an important limiting case to the $Na_2O$-$Al_2O_3$-$SiO_2$ phase diagram at high pressure and accounts for excess Si components in sodic high-pressure pyroxenes.

Albitic jadeite is ~21% denser than albite and lingunite is ~11% denser than albitic jadeite. The geometry of the T site of albitic jadeite is the same as in endmember jadeite. The structure refinement of albitic jadeite from Ries, however, suggests that the M2 site is slightly contracted and the M1 site expanded due to the incorporation of Si. M2 contraction is mostly along the longest M2-O2 bond vector, whereas it is nearly equal for the other bond vectors (Table S3).

## IMPLICATIONS

Albitic jadeite occurs in terrestrial and meteoritic shock-metamorphic parageneses at pressures between 18 and 22 Gpa, formed under conditions similar to lingunite. The larger molar volume of albitic jadeite compared to lingunite suggests that it forms along a transformation sequence controlled by the Ostwald step rule: albitic maskelynite → albitic jadeite → lingunite. The value of the Ostwald step rule for interpreting shock metamorphic phase transitions has been pointed out previously (e.g., Tschauner et al. 2021).

Albitic jadeite does not occur in the matrix of shock-melt veins other than as clasts. Figure 1 shows that the melt vein matrix contains only garnet with a sodic component in accordance with the substitution mechanism Na + Si → Mg + Al, corresponding to a hypothetical endmember $(Na_2Ca)Si_2Si_3O_{12}$. Hence, clinopyroxene within shock-melt vein matrices is generally expected to be jadeite and not albitic jadeite. On the other hand, it is likely that maskelynite of albite-rich composition transforms around shock melt veins or pockets into the vacancy-stabilized clinopyroxenes described here.

The molar volume of albitic jadeite is 73.63 ±1.09 $cm^3$/mol for the composition range $(Na_{0.75}\square_{0.25})(Al_{0.75}Si_{0.25})Si_2O_6$ to $(Na_{0.50}Ca_{0.25}\square_{0.25})AlSi_2O_6$, which is substantially larger than the volume of the decompositon products of the reaction albite → jadeite + coesite (V = 69.65 $cm^3$/mol). The difference of 4 $cm^3$/mol likely accounts for the stability of jadeite + coesite over albitic jadeite. However, there is a more fundamental point that can be taken from the volume difference: Albitic jadeite falls within a distinct trend of pressure-induced volume relations which involve metastable high-pressure phases or significant configurational entropy and which follow the relation $\Delta V \approx 3 \cdot \exp[(\Delta V'/15]$. In the present case, $\Delta V$ is the volume difference between albite and clinopyroxene and $\Delta V'$ the difference between albite and lingunite, respectively, all taken at ambient reference conditions (Tschauner 2020). The relation gives $\Delta V = 16.87 \pm 1.1$ (observed) ~ $15.9 \pm 1.7$ (calculated) $cm^3$/mol. Neither albitic jadeite nor lingunite has a stability field, which is consistent with the underlying causes of this relation (Tschauner 2020). In contrast, tissintite exhibits a 10% smaller volume than the decomposition products grossular, zagamiite, and kyanite (Liu et al. 2012, Tschauner 2020). The Ca-Eskola component, which characterizes tissintite, is found as a minor component in eclogitic clinopyroxene (McCormick 1986), whereas the albitic pyroxene component is preferrentially dissolved in garnet in subducted MORB at pressures

where albitic jadeite forms in impactites. These garnets were originally described as garnets with excess pyroxene component (Moore and Gurney 1985) based on their composition. Structurally, they are characterized by a majoritic component and Na on the X-site, both clearly correlated with pressure (Collerson et al. 2010, Wijbrans et al. 2016).

## ACKNOWLEDGEMENTS

SEM, EDS, EBSD and EPMA analyses were carried out at the Caltech GPS Division Analytical Facility, which is supported, in part, by NSF Grants EAR-0318518 and DMR-0080065. OT acknowledges support by NSF EAR-1838330. YL thanks the supports by the Leader Researcher program (NRF-2018R1A3B1052042) of the Korean Ministry of Science, ICT and Planning and PE20200 funded by the Korea Polar Research Institute. GSECARS is supported through DOE Award DESC0005278, and NSF awards EAR-1128799,-0318518, DE-FG02-94ER14466, and DMR-0080065. The Advanced Photon Source, a DOE Office of Science User Facility, is operated by Argonne National Laboratory under Contract No. DE-AC02-06CH11357. We thank V. Stähle and M. Trieloff for providing material of the Ries xenolith thin section ZLN100 for this study, Chang-kun Park of Korea Polar Research Institute for providing TIL 08001, and D. Stöffler for stimulating discussions.

## REFERENCES

Angel, R.J., Gasparik, T., Ross, N.L., Finger, L.W., Prewitt, C.T., and Hazen, R.M. (1988) A silica-rich sodium pyroxene phase with six-coordinated silicon. Nature, 335, 156–158.

Bell, D.R. and Rossman, G.R. (1992) Water in the Earth's mantle: the role of nominally anhydrous minerals. Science, 255, 1391–1397.

Collerson, K.D., Williams, Q., Kamber, B.S., Omori, S., Arai, H., and Ohtani, E. (2010). Majoritic garnet: A new approach to pressure estimation of shock events in meteorites and the encapsulation of sub-lithospheric inclusions in diamond. Geochimica et Cosmochimica Acta, 74, 5939–5957.

Gillet, P., Chen, M., Dubrovinsky, L., and El Goresy, A. (2000) Natural $NaAlSi_3O_8$-hollandite in the shocked Sixiangkou meteorite. Science, 287, 1633–1636.

Hatert, F. and Burke E.A.J. (2008) The IMA-CNMNC dominant-constituent rule revisited and extended. Canadian Mineralogist, 46, 717–728.

Huang, S., Tschauner, O., Yang, S., Humayun, M., Liu, W., Gilbert Corder, S.N., Hans A. Bechtel, H.A., and Tischler, J. (2020) HIMU geochemical signature originating from the transition zone. Earth and Planetary Science Letters, 542, 116323.

Larson, A.C. and von Dreele R.B. (2004) General Structure Analysis System (GSAS), Los Alamos National Laboratory Report LAUR 86-748.

Liou, J.G. Zhang, R.Y., Ernst, W.G., Rumble III, D. and Maruyama, S. (1998) High-pressure minerals from deeply subducted metamorphic rocks. In R.J. Hemley, Ed.,Ultrahigh-pressure Mineralogy, Physics and Chemistry of the Earth Deep Interior, 37, 33–196. Reviews in Mineralogy, Mineralogical Society of America, Washington, D.C.

Liu, L.-G. (1978) High-pressure phase transformations of albite, jadeite and nepheline. Earth and Planetary Science Letters, 37, 438–444.

Liu, X., Ohfuji, H., Nishiyama, N., He, Q., Sanehira, T., and Irifune, T. (2012) High-P behavior of anorthite composition and some phase relations of the $CaO$-$Al_2O_3$-$SiO_2$ system to the lower mantle of the Earth, and their geophysical implications. Journal of Geophysical Research Solid Earth, 117, Article Number: B09205.

Ma, C., Tschauner, O., Beckett, J.R., Liu, Y., Rossman, G.R., Zhuravlev, K., Prakapenka, V., Dera, P., and Taylor, L.A. (2015) Tissintite, $(Ca,Na,\square)AlSi_2O_6$, a highly-defective, shock-induced, high-pressure clinopyroxene in the Tissint martian meteorite. Earth and Planetary Science Letters, 422, 194–205.

Ma, C., Tschauner, O., Kong, M., Beckett, J.R., Greenberg, E., Prakapenka, V.B., Lee, Y. (2020) Discovery of a highly-defective, shock-induced, high-pressure albitic jadeite, $(Na,Ca,\square_{1/4})(Al,Si)Si_2O_6$: Natural occurrence of a clinopyroxene with excess Si. 51st Lunar and Planetary Science Conference, Abstract no. 1712.

McCormick, T.C. (1986) Crystal-chemical aspects of nonstoichiometric pyroxenes. American Mineralogist, 71, 1434–1440.

Miyahara, M., Ozawa, S., Ohtani, E., Kimura, M., Kubo, T., Sakai, T., Nagase, T., Nishijima, M., and Hirao, N. (2013) Jadeite formation in shocked ordinary chondrites. Earth and Planetary Science Letters, 373, 102–108.

Moore, R.O. and Gurney, J.J. (1985) Pyroxene solid solution in garnets included in diamond. Nature, 318, 553-555.

Prescher, C. and Prakapenka, V.B. (2015) DIOPTAS: a program for reduction of two-dimensional X-ray diffraction data and data exploration. High Pressure Research, 35, 223-230.

Sharp, T.G. and DeCarli, P.S. (2006) Shock effects in meteorites. In Meteorites and the early solar system II, edited by Lauretta D. S. and McSween H. Y. Jr. Tucson, Arizona: University of Arizona Press. pp. 653–677.

Stähle, V., Altherr, R., Nasdala, L., and Ludwig, T. (2011) Ca-rich majorite derived from high-temperature melt and thermally stressed hornblende in shock veins of crustal rocks from the Ries impact crater (Germany). Contributions to Mineralogy and Petrology, 161, 275–291.

Stähle, V., Altherr, R., Nasdala, L., Trieloff, M., and Varychev, A. (2017) Majoritic garnet grains within shock-induced melt veins in amphibolites from the Ries impact crater suggest ultrahigh crystallization pressures between 18 and 9 GPa. Contributions to Mineralogy and Petrology, 172, Article number: 86; DOI 10.1007/s00410-017-1404-7.

Tropper, P., Essene, E.J., Sharp, Z.D., and Hunziker, J.C. (1999) Application of K-feldspar–jadeite–quartz barometry to eclogite facies metagranites and metapelites in the Sesia Lanzo Zone (Western Alps,Italy). Journal of metamorphic Geology, 17, 195–209.

Tschauner, O., Ma, C., Lanzirotti, A. and Newville, M.G. (2019) Riesite, a new high pressure polymorph of $TiO_2$ from the Ries impact structure. 10, 78; doi:10.3390/min10010078.

Tschauner, O. (2020) Empirical constraints on volume changes in pressure-induced solid state transformations. High Pressure Research, 40, 511-524.

Tschauner, O., Ma, C., Spray, J.G., Greenberg, E. and Prakapenka, V.B. (2021) Stöfflerite, $(Ca,Na)(Si,Al)_4O_8$ in the hollandite structure: A new high-pressure polymorph of anorthite from martian meteorite NWA 856. American Mineralogist, 106, 650–655.

Warren, J.M. and Hauri, E.H. (2014) Pyroxenes as tracers of mantle water variations. Journal of Geophysical Research - Solid Earth, 119, 1851–1881.

Wijbrans, C.H., Rohrbach A., and Klemme, S. (2016) An experimental investigation of the stability of majoritic garnet in the Earth's mantle and an improved majorite geobarometer. Contributions to Mineralogy and Petrology, 171, 50.

Wood, B.J. and Henderson, C.M.B. (1978) Compositions and unit-cell parameters of synthetic non-stoichiometric tschermakitic clinopyroxenes. American Mineralogist, 63, 66–72.

Yang, H., Konzett, J., Frost, D.J., and Downs, R.T. (2009) X-ray diffraction and Raman spectroscopic study of clinopyroxenes with six-coordinated Si in the $Na(Mg_{0.5}Si_{0.5})Si_2O_6$-$NaAlSi_2O_6$ system. American Mineralogist, 94, 942–949.

Zhang, L., Song, S., Liou, J.G., Ai, Y., and Li, X. (2005) Relict coesite exsolution in omphacite from Western Tianshan eclogites, China. American Mineralogist, 90, 181–186.

356 **Table 1**. EPMA data for albitic jadeite and garnet in a melt vein and nearby albite from Ries.
357

| Constituent | albitic jadeite | | garnet | | albite | |
|---|---|---|---|---|---|---|
| wt% | n=7[a] | SD[c] | n=5 | SD | n=4 | SD |
| $SiO_2$ | 65.97 | 1.99 | 45.99 | 1.35 | 67.95 | 0.31 |
| $TiO_2$ | b.d.[b] | | 0.93 | 0.12 | b.d. | |
| $Al_2O_3$ | 20.51 | 0.77 | 16.65 | 1.65 | 20.09 | 0.23 |
| FeO | 0.51 | 0.15 | 11.70 | 1.39 | 0.45 | 0.04 |
| MgO | 0.14 | 0.12 | 8.35 | 0.76 | 0.02 | 0.02 |
| CaO | 1.11 | 0.19 | 10.15 | 2.08 | 0.83 | 0.28 |
| $Na_2O$ | 10.05 | 0.96 | 2.29 | 0.42 | 11.10 | 0.16 |
| $K_2O$ | 0.85 | 0.25 | 0.27 | 0.04 | 0.19 | 0.12 |
| $Cr_2O_3$ | b.d. | | b.d. | | b.d. | |
| MnO | b.d. | | 0.19 | 0.02 | b.d. | |
| Total | 99.16 | | 96.53 | | 100.63 | |
| | | | | | | |
| No. O atoms | 6 | | 12 | | 8 | |
| Si | 2.19 | | 3.48 | | 2.96 | |
| Ti | | | 0.05 | | | |
| Al | 0.80 | | 1.49 | | 1.03 | |
| Fe | 0.01 | | 0.74 | | 0.02 | |
| Mg | 0.01 | | 0.94 | | 0.00 | |
| Ca | 0.04 | | 0.82 | | 0.04 | |
| Na | 0.65 | | 0.34 | | 0.94 | |
| K | 0.04 | | 0.03 | | 0.01 | |
| Cr | | | | | | |
| Mn | | | 0.01 | | | |
| Cation sum | 3.74 | | 7.90 | | 5.00 | |

358 [a] n = number of analyses.
359 [b] b.d. = below detection limit, 0.02 wt% for Ti, 0.03 wt% for Cr, and 0.02 wt% for Mn.
360 [c] SD = standard deviation. Errors are one standard deviation of the mean based on all of the
361 analyses.

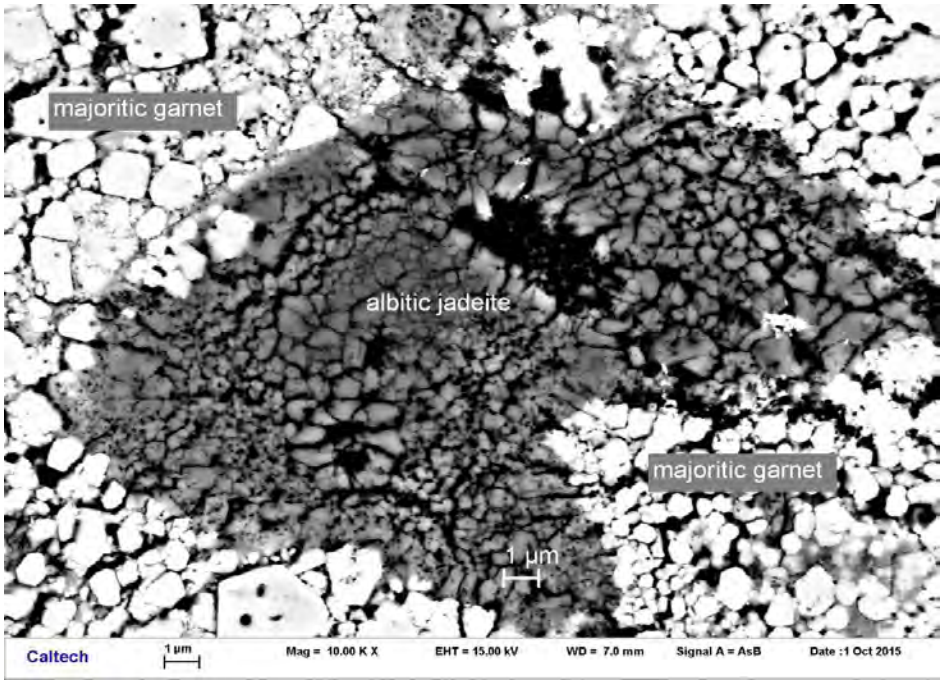


**Figure 1**. Backscatter electron (BSE) image showing albitic jadeite with euhedral garnet within a shock-melt vein in an amphibolite xenolith from Ries impact crater.

(a) TIL 08001

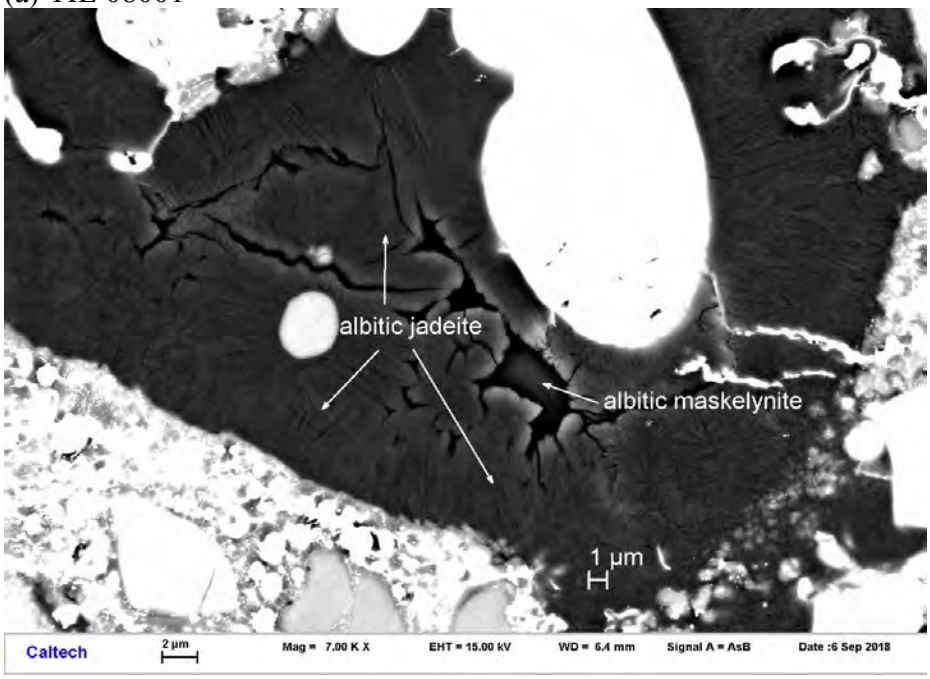


(b) EET 13014

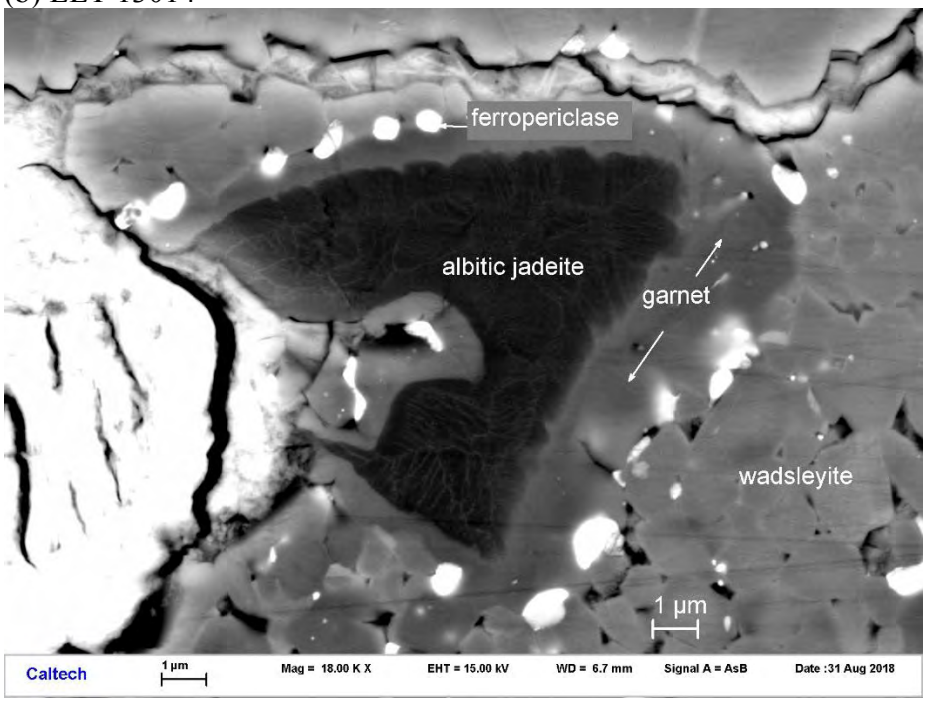

This is the peer-reviewed, final accepted version for American Mineralogist, published by the Mineralogical Society of America.
The published version is subject to change. Cite as Authors (Year) Title. American Mineralogist, in press.
DOI: https://doi.org/10.2138/am-2021-7925. http://www.minsocam.org/

(c) EET 13052

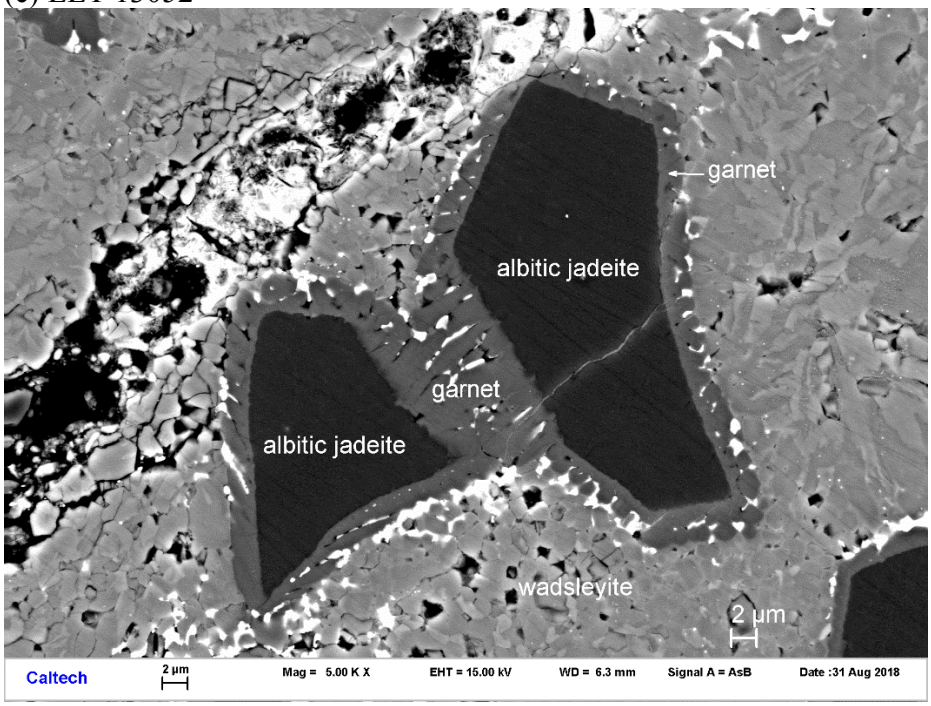


(d) NWA 1662

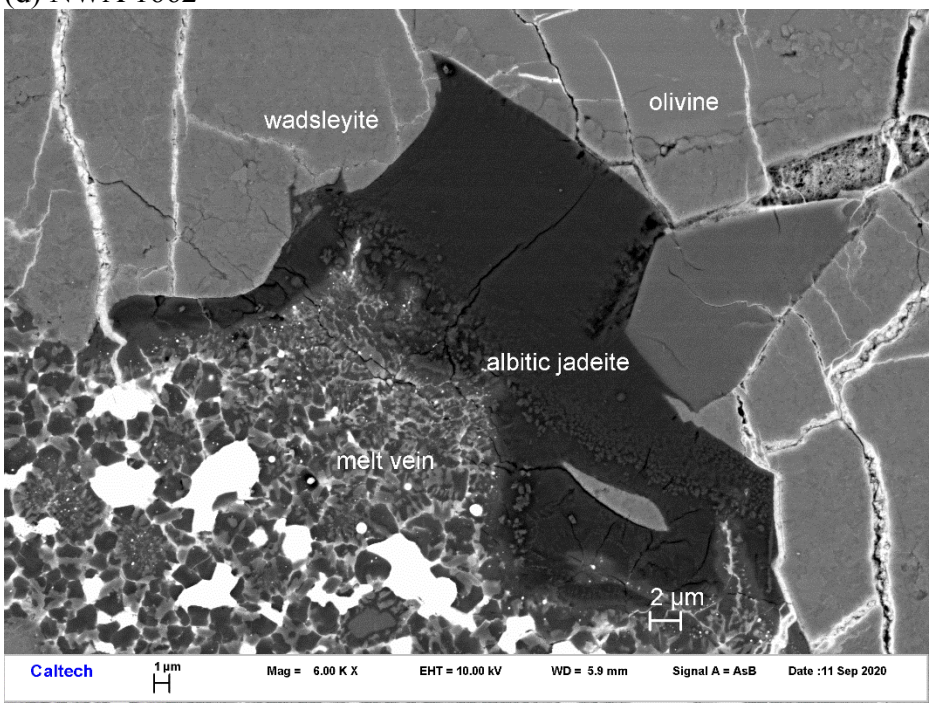


**Figure 2**. BSE images showing albitic jadeite formed from maskelynite in shock-melt veins from the L6 ordinary chondrites (a) TIL 08001, (b) EET 13014, (c) EET 13052, and (d) NWA 1662.

This is the peer-reviewed, final accepted version for American Mineralogist, published by the Mineralogical Society of America.
The published version is subject to change. Cite as Authors (Year) Title. American Mineralogist, in press.
DOI: https://doi.org/10.2138/am-2021-7925. http://www.minsocam.org/

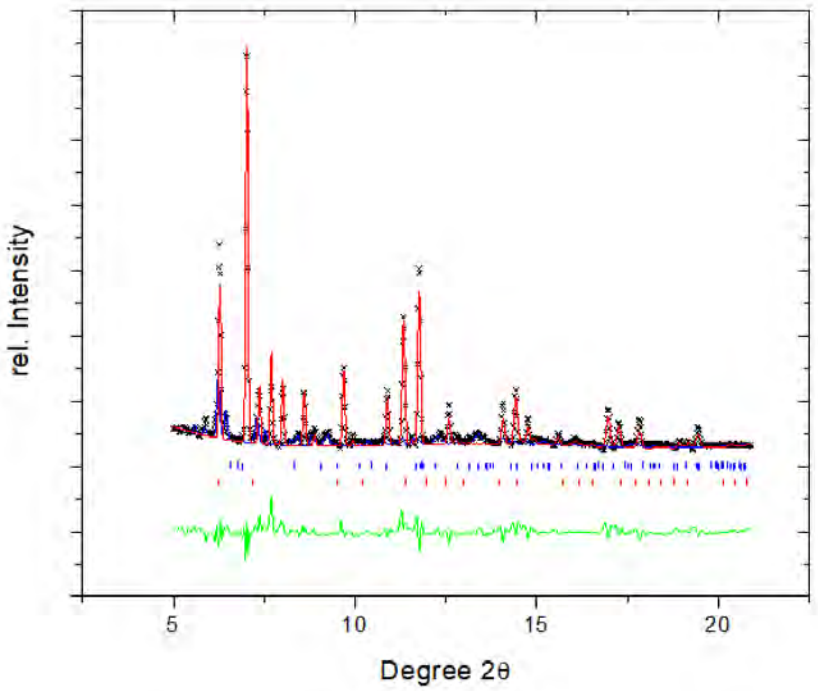


**Figure 3**. Powder X-ray diffraction pattern of albitic jadeite and garnet in the shock-melt vein of section ZLN100 from the Ries impact crater (Fig. 1). Black crosses: observed pattern, red line: Rietveld refinement, green line: residual. Blue and red tickmarks are the positions of the observable reflections of albitic jadeite and garnet, respectively. The X-ray wavelength was 0.31856 Å.

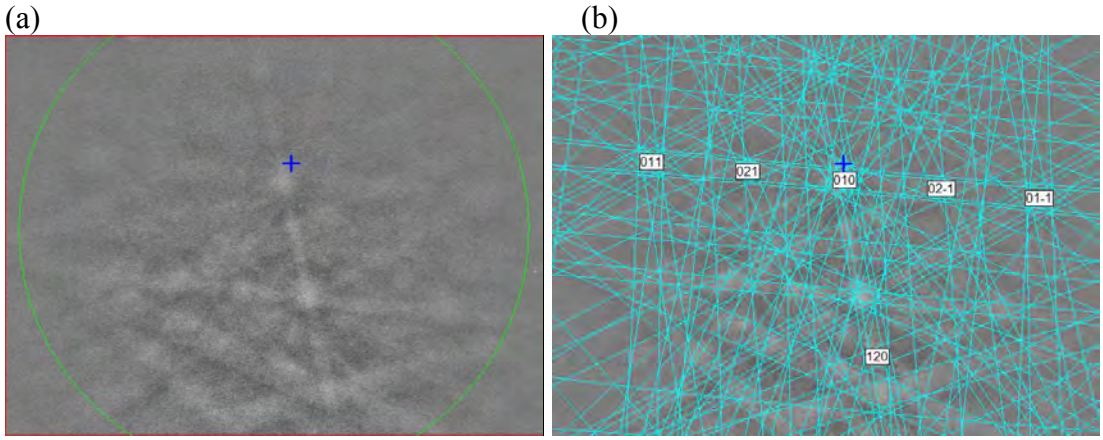


**Figure 4**. (a) EBSD pattern of an albitic jadeite crystal in NWA 1662, (b) indexed to a *C*2/*c* diopside-type structure.